

Tackle Your Sample Preparation, Amplification and Analysis Challenges

Learn helpful tips, tricks & technique refreshers with our free eBook

Looking for a quick technique refresher or a way to support your mentee? Need to adapt an existing technology or need a unique formulation, but not sure where to start? Our Custom Solutions eBook can help.

This eBook was designed as an educational resource to address your sample preparation, amplification and analysis challenges in the lab. It also offers insight into the benefits and value of partnering with a Custom/OEM supplier.



To Download the Free eBook, Scan the QR Code or Visit:

www.promega.com/CustomSolutionsEbook





ARTICLE



Multi-information source Bayesian optimization of culture media for cellular agriculture

²Operations Research and Information Engineering, Cornell University, Ithaca, New York, USA

³Departments of Neurobiology, Physiology, and Behavior and Physiology and Membrane Biology, University of California Davis, Davis, California, USA

⁴Department of Viticulture and Enology, University of California, Davis, USA

Correspondence

David E. Block, Department of Viticulture and Enology, University of California, Davis, CA, USA.

Email: deblock@ucdavis.edu

Funding information

New Harvest; Good Food Institute; National Science Foundation, Grant/Award Number: 2021132

Abstract

Culture media used in industrial bioprocessing and the emerging field of cellular agriculture is difficult to optimize due to the lack of rigorous mathematical models of cell growth and culture conditions, as well as the complexity of the design space. Rapid growth assays are inaccurate yet convenient, while robust measures of cell number can be time-consuming to the point of limiting experimentation. In this study, we optimized a cell culture media with 14 components using a multiinformation source Bayesian optimization algorithm that locates optimal media conditions based on an iterative refinement of an uncertainty-weighted desirability function. As a model system, we utilized murine C2C12 cells, using AlamarBlue, LIVE stain, and trypan blue exclusion cell counting assays to determine cell number. Using this experimental optimization algorithm, we were able to design media with 181% more cells than a common commercial variant with a similar economic cost, while doing so in 38% fewer experiments than an efficient design-of-experiments method. The optimal medium generalized well to long-term growth up to four passages of C2C12 cells, indicating the multi-information source assay improved measurement robustness relative to rapid growth assays alone.

KEYWORDS

Bayesian optimization, cellular agriculture, expected improvement, Gaussian process, media optimization, multi-information source

1 | INTRODUCTION

Every bioprocess in which cells are the final product or used in the production process requires suitable culture conditions for cell growth and product quality. In the rapidly growing cellular agriculture/cultivated meat industry, where cells are grown for consumption to replace carbon-intensive and often unethical animal agriculture, cost-effective media has been identified as the most critical aspect in scale-up and commercialization (O'Neill et al., 2021). Optimizing

these conditions is difficult due to a large number of media components with nonlinear and interacting effects between cells, medium, matrix material, and reactor environment (Brunner et al., 2010). Typically, culture media used for processes in cellular agriculture consist of a basal medium of glucose, amino acids, vitamins, and salts (such as the common Dulbecco's Modified Eagle Medium [DMEM]) supplemented with fetal bovine serum (FBS) for improved cell survival. FBS is an undefined, animal-derived serum consisting of proteins, hormones, and other large molecular weight

This is an open access article under the terms of the Creative Commons Attribution-NonCommercial-NoDerivs License, which permits use and distribution in any medium, provided the original work is properly cited, the use is non-commercial and no modifications or adaptations are made.

© 2022 The Authors. Biotechnology and Bioengineering published by Wiley Periodicals LLC.

¹Department of Chemical Engineering, University of California Davis, Davis, California, USA

components, and contributes substantially to the cost of media (van der Valk, 2018). Even when enriched with additional growth factors or FBS, media is often far from optimal for all cell types and requires adaptation and/or optimization (Kolkmann et al., 2020), which is difficult for media mixtures with >30 components, as is common in cell culture.

To manage this complexity, design-of-experiments (DOE) methods are often employed in which factors (concentrations or environmental conditions) are set to a user-specified value (usually "high" or "low") and outputs are measured (Singh et al., 2017; Zhang & Mills, & Block, 2009). These DOE designs are arranged in such a way that statistically meaningful correlations can be found in fewer experiments than techniques like intuition, "one-factor-at-a-time" sequences, or random designs. A more advanced form of this is to use sequential, model-based DOEs such as a radial basis function (Cosenza & David, 2020; Zhang & Block, 2009; Zhang et al., 2007) or Gaussian Process (GP) (Kotthoff et al., 2021), combined with an optimizer/sampling policy, to automatically select sequences of optimal designs. These approaches are often more efficient than traditional DOE at optimizing systems using fewer experiments (Cosenza et al., 2021) and allow for more natural incorporation of process priors (Coleman & Block, 2006), measurement noise (Ankenman et al., 2010; Tracey & Wolpert., 2018), probabilistic output constraints and constraint learning (Letham et al., 2019), multiobjective (Belakaria et al., 2019), multipoint (Wang et al., 2020), and multi-information source designs (Jian & Frazier, 2018; Shu et al., 2021: Takeno et al., 2019).

Even with these methods available, limitations still exist. In previous work, we applied a machine learning approach to optimize complex media design spaces but had limited success due to the difficulty in measuring cell number for multipassage growth (Cosenza et al., 2021). Therefore, in this study, we utilized a multi-information source (IS) Bayesian model to fuse "cheap" measures of cell biomass (rapid chemical assays which can be done at scale) with more "expensive" but higher quality measurements (cell numbers over time which represents a high-quality metric of growth media quality) to predict long-term medium performance. We refer to the simpler and cheap assays as "low-fidelity" IS, and more complex and expensive assays as "high-fidelity" IS. While not always predictive of long-term growth, these lower fidelity assays are at least correlated with cell health and can help in identifying interesting regions of the design space for further study with the high-fidelity IS. We used this model, with Bayesian optimization (BO) tools, to optimize a cell culture medium with 14 components while minimizing the number of experiments, optimally allocating laboratory resources, and building process knowledge to improve our optimization scheme and model. In Section 2 we discuss the computational and experimental components of this BO method. In Section 3 we present the results of the BO method in comparison to a traditional DOE method, followed by Section 4 where we demonstrate the importance of fusing multiple sources of information to obtain relevant process knowledge and/or optimization results.

2 | METHODS

2.1 | Cells and media components

The system under consideration was the proliferation of C2C12 (ATCC) cells. These cells are immortalized muscle cells with similar metabolism and growth characteristics as other adherent cell lines useful in the cellular agriculture industry. Cells were stored in 70% DMEM (Gibco), 20% FBS (BioWest), 10% dimethyl sulfoxide (Thermo Fischer) freeze medium at -196°C until thawed. Vials were thawed to 25°C and the freezing medium was removed by centrifugation at 1500 g for 5 min. The centrifuged cell pellet was resuspended in 17 ml of DMEM with 10% FBS and placed on 15 cm sterile plastic tissue culture dishes (at about 10⁶ cells/plate) (Cellstar, Greiner Bio-One). Cells were incubated in a 37°C and 5% CO₂ environment. After 24 h the medium was removed, the culture dish-washed with Phosphate Buffer Solution (PBS) (Gibco), and fresh DMEM with 10% FBS was introduced. After an additional 24 h, cells were harvested using tripLE solution (Gibco), diluted in PBS, and counted using Countess II with trypan blue exclusion and disposable slides (Invitrogen). The process of removing cells from a plate, counting, and re-plating them with fresh medium is called subculturing or passaging. How well the C2C12 cells survive and grow after passaging is indicative of their long-term potential in a large cellular agriculture process.

The design space was comprised of the components and minimum/maximum concentrations listed in Table 1. These components were chosen because they are often used to supplement standard DMEM to improve cell growth; this represents a reasonable test case for the industrial application of these multi-IS BO methods to the cellular agricultural industry. The composition of standard DMEM (such as the medium used above), is shown in Table 3, and should not be confused with the base DMEM "supplement" (Gibco), which contains only amino acids, trace metals, salts, and vitamins and none of the other 14 components. pH and osmolarity are not controlled in this study, so act as latent variables.

2.2 | Cell growth experiments and assays

For the high-fidelity IS, 750 μ I of cell suspension containing 60,000 cells were placed in a six well plate (three replicates) with 2.25 ml of the test medium. For low-fidelity IS, 25 μ I of cell suspension containing 2000 cells were placed in 96 well plates (four replicates and two control wells without cells) with 75 μ I of the test medium. All experiments thus had 6250 cells/cm² and 312.5 ml/cm² of media. After 72 h, all wells were measured using the IS methods shown in Table 2.

The AlamarBlue assay required staining wells with 10% v/v (10 μ l) AlamarBlue stock solution (Invitrogen), 4 h of incubation in a 37°C and 5% CO₂ incubator, and measurement of 570 λ_{570} nm and 600 nm λ_{600} absorbance wavelengths (Molecular Devices, ImageX-press Pico) as well as the control wells $\lambda_{570,c}$ and $\lambda_{600,c}$ (no cells) to get AlamarBlue reduction metric %AB.

TABLE 1 Media components.

Abrev.	Component	Conc. min (mg/ml)	Conc. Max (mg/ml)	Cost	Use in cell culture	
T	Transferrin	0	0.026	6.53E-03	Iron transport, homeostasis	
1	Insulin	0	0.035	1.43E-02	GF for glucose and amino acid utilization	
SS	Sodium selenite	0	1.75E-05	6.4E-09	Chemical pathways	
AA	Ascorbic acid	0	8.75E-03	9.8E-06	Antioxidant	
Glu	Glucose	0	15.75	0.2	Carbon source	
Gluta	Glutamine (GlutaMAX)	0	1.519	2.09E-02	Carbon source	
Albu	Albumin (AlbuMAX)	0	1.4	4.94	Stabilization of small molecules	
FBS	FBS (% v/v)	0	17.5	14.00	Shear protection, cytokines, other	
Н	Hydrocortisone	0	1.75E-05	1.1E-05	Proliferation, differentiation, inhibition	
D	Dexamethasone	0	7.00E-04	7.2E-03	Short-term proliferation, muscle breakdown	
Р	Progesterone	0	1.75E-05	4.0E-07	Proliferation	
Esd	Estradiol	0	8.75E-06	1.6E-06	Proliferation	
Ethan	Ethanolamine	0	6.65E-03	6.1E-06	Phospholipid synthesis	
Glutath	Glutathione	0	3.50E-03	6.0E-04	Antioxidant, thiol chemical pathways	
-	DMEM supplement (% v/v)	-	***54.3	2.1E-02	Amino acids, vitamins, salts, buffer	

Note: All components are shown were stored as per manufacturers (PreproTech unless specified) instructions in stock solutions. The concentration (mg/ml) of all media was between the minimum and maximum listed. The cost shown is a unitless scalarization of the relative economic cost of each component.

Abbreviations: DMEM, Dulbecco's modified Eagle's medium; FBS, fetal bovine serum.

***All media have a 54.3% v/v (volume percent) base of DMEM supplement (liquid form, no glucose, glutamine, or FBS). Remaining volume (minus component volumes) was made up in water.

TABLE 2 Information sources for cell number measurement.

Information source	Time required	Format	Mechanism of action	
Passage 2 (high-fidelity)	6 Days	6 Wells	Trypsinization/trypan blue exclusion	
Passage 1***	3 Days	6 Wells	Trypsinization/trypan blue exclusion	
AlamarBlue (low-fidelity)	3 Days	96 Wells	Mitochondria activity/colorimetric	
LIVE Stain (low-fidelity)	3 Days	96 Wells	Nuclear/fluorometric	

Note: These sources of information (IS) were used to approximate and model C2C12 cell number. In this study, Passage 2 cell numbers were considered the highest-fidelity IS, while AlamarBlue and the LIVE stains were the lowest.

***Passage 1 cell number measurements were necessary to get Passage 2, so were included as a separate IS. Every high-fidelity IS measurement of a medium was also made in parallel with a low-fidelity measurement. Their inter-IS correlations are shown in Figure 8c.

$$\% AB = \frac{117216 \times \lambda_{570} - 80586 \times \lambda_{600}}{155677 \times \lambda_{600,c} - 14652 \times \lambda_{570,c}}.$$

The LIVE assay required that the test wells be washed with PBS, and $100\,\mu l$ of $1\,\mu M$ LIVE stain Calcein AM (Biotium) be introduced into the test wells and incubated for $1.5\,h$ at $37^{\circ}C$ and 5% CO $_2$. The biomass/cell number correlates was then measured using a fluorometer (Molecular Devices, ImageXpress Pico) at Ex/Em 494/530 fluorescein filters and calculated using the emission F_{530} . Both LIVE and %AB metrics are correlated with cell number and thus were the

low-fidelity IS metric of cell number.

LIVE =
$$F_{530}$$
.

We also measured the cell number using an automatic cell counter (Counters II) with trypan blue exclusion. This required trypsinization outlined in the previous section. Because we wished to measure long-term cell viability, after the first cell count (Passage 1), we re-seeded the cells under the same conditions and measured the cell count after an additional 72 h (Passage 2). The Passage 2 metric incorporated long-term viability and the effect of trypsinization, and thus was the most robust measurement of cell number. All measurements/correlates of cell number (%AB, LIVE, cell number)

TABLE 3 Optimal media.

Abrev.	Component conc. (mg/ml)	ВО	DOE	DMEM (control)
Т	Transferrin	2.16E-02	0	0
1	Insulin	2.27E-02	0	0
SS	Sodium selenite	6.34E-06	0	0
AA	Ascorbic acid	0	0	0
Glu	Glucose	8.97	6.75	4.50
Gluta	Glutamine (GlutaMAX)	1.32	0.65	0.43
Albu	Albumin (AlbuMAX)	0	0	0
FBS	FBS (% v/v)	10.1	7.5	10.0
Н	Hydrocortisone	0	0	0
D	Dexamethasone	0	0	0
Р	Progesterone	1.75E-05	0	0
Esd	Estradiol	8.75E-06	0	0
Ethan	Ethanolamine	3.64E-03	0	0
Glutath	Glutathione	2.49E-03	0	0
-	DMEM supplement (% v/v)	54.3	54.3	54.3
	Outputs (dimensionless)			
	Num. experiments	81	133	-
D(x)	Desirability	0.94	0.40	0.44
y(x)	Proliferation metric	2.82	0.86	1.00
c(x)	Cost metric	8.22	6.12	8.09

Note: Concentrations (mg/ml) of best BO-designed medium alongside that found by DOE and the DMEM control used throughout this study. The resulting objective function D(x), cell number y(x), and cost c(x) of each medium are shown with the required number of experiments to get the optimal result.

Abbreviations: BO, Bayesian optimization; DMEM, Dulbecco's modified Eagle's medium; DOE, design-of-experiments; FBS, fetal bovine serum.

were reported as ratios, normalized to the DMEM control (whose concentration is shown in Table 3).

2.3 DOE method

To compare our BO method to a typical method used in the optimization of fermentation/bioprocess systems (Singh et al., 2017; Zhang & Mills, & Block, 2009), we used a DOE. We first screened all 14 components using a folded Plackett-Burman (PB) design (which is a normal PB combined with an additional PB design with "high" factors set to "low" and vice versa) using the AlamarBlue IS. A linear model $D(x) = \beta_0 + \sum_{i=1}^{p} x_i \beta_i$ let us quantify the desirability of each component using the slope β_i (desirability D(x) will be talked about in Section 2.4.2). The lower bound of the PB was set to x = 0 (0 mg/ml) and the upper bound x = 0.28 (28% of maximum concentration shown in Table 1, for example, glucose would be set to

 $0.28 \times 15.75 \,\text{mg/ml} = 4.41 \,\text{mg/ml}$) so that component quality could first be judged at modest concentration where nonlinear effects would be minimal. We then set unimportant or harmful $(\beta_i \le 0)$ components to x = 0 for the rest of the DOE study, then ran a Box-Behnken (BB) design over the remaining useful components using AlamarBlue IS. The BB was used to estimate an interactionpolynomial model $D(x) = \beta_0 + \sum_{i=1}^p x_i \beta_i + \sum_{i=1}^p x_i^2 \beta_i + \sum_{1 \le i \le i} x_i x_i \beta_{i,i}$ and a multistart Newton's Method was used to find the D(x)-optimal concentrations inside the design space. If the optimal concentrations were found to be on any edge of the current BB, then the bounds of the design were shifted $\Delta x = 0.145$ dimensionless units in that direction (steepest accent) and another BB was run using these new bounds. This was done because the optimal boundary of the design space is uncertain and needed to be found. The sequential BB was run until the optimal bounds were found or resources exhausted. The best medium was then reported as the optimal point found using multistart Newton's Method within the final optimal bounds.

2.4 BO method

2.4.1 | Bayesian model

In standard BO, a function g is modeled using a Gaussian Process (GP) (Poloczek et al., 2017), characterized by a prior mean μ_0 and covariance Σ , with the property that for any X finite collection of N points with dimensionality p, the prior distribution of the output g(X) is normal $g(X) \sim N(\mu_0, \Sigma(X, X))$. The prior determines the directionality and "wigglyness" of the function through the covariance kernel function Σ , which models the relationship between any two points x and x'. We chose the squared exponential function for the kernel to encode the belief that (i) similar experiments are more alike than dissimilar experiments governed by hyperparameters σ_f^2 and $\lambda_{1\dots p}^2$ and (ii) that the overall biological processes underlying the response surface are smooth with (iii) each component response governed by λ_k^2 , allowing each component k to have different degrees of "wigglyness."

$$\Sigma(x, x') = \sigma_f^{2*} exp\left(-1/2\sum_{k=1}^{p} (x_k - x_k')^2/\lambda_k^2\right).$$
 (1)

If we collect N observations of inputs $X_N = [x_1...x_N]$ and outputs $Y_N = [y_1...y_N]$ from the generative process $y(x) = g(x) + \epsilon$ we can get the posterior distribution $g(x) \mid X_N, Y_N \sim N(\mu(X_N), \Sigma(X_N, X_N))$ where the mean and variance of g(x) are given by Equations (2) and (3) respectively for homoscedastic noise $\Sigma_\epsilon = \sigma_\epsilon^{2*}I$ with process noise variance σ_ϵ^2 .

$$\mu(x) = \mu_0 + \sum (X_N, x)(\sum (X_N, X_N) + \sum_{\epsilon})^{-1}(Y_N - \mu_0), \tag{2}$$

$$\sigma^2(x) = \Sigma(x, x) - \Sigma(X_N, x)(\Sigma(X_N, X_N) + \Sigma_c)^{-1}\Sigma(X_N, x)^T.$$
 (3)

A more detailed discussion of GP models can be found in (Schulz et al., 2018). With a predictive model of the mean $\mu(x)$ and variance

 $\sigma^2(x)$ of cell number, we can use past experimental data inputs X_N and outputs Y_N to inform future process optimization.

The key objective of this study was to maximize C2C12 cell growth/accumulation while minimizing media costs. To do this, measuring cell growth was critical but experimentally expensive. Less expensive assays can approximate cell growth, yet with reduced accuracy. Therefore, it was beneficial to use combinations of cell growth assays to facilitate experimentation while decreasing the overall experimental burden. This provides a balance between quality of information and experimental cost. To this end we adopted the multi-information source GP model introduced by (Poloczek et al. (2017), which utilizes auxiliary information sources to model an underlying "true" function. We chose this model over the more typical multi-task GP to encode the prior belief that the generative model includes an underlying "true" function and several biased/ variable but correlated auxiliary functions, and to provide the flexibility of allowing different length-scale hyperparameters λ_k for each IS to be learned from the data.

Let us assume a generative model $y = g(x) + \delta(x, m) + \epsilon$ for a given medium combination x at an IS indexed by m. We, therefore, have one independent GP for the underlying function g(x) and one for each auxiliary IS deviation function $\delta(x, m)$ for the m th auxiliary IS (where m = 0 references the underlying IS). To implement this, Equation (1) is modified by adding an additional kernel (squared exponential) to the original kernel anytime an auxiliary datapoint $m \neq 0$ is referenced and x and x' have the same IS index using an indicator function $\mathbf{1}_{m\neq 0}\mathbf{1}_{m=1}$.

$$\Sigma(x_m, x_l') = \Sigma_{O(x, x')} + \mathbf{1}_{m \neq 0} \mathbf{1}_{m = l} \Sigma_m(x, x'). \tag{4}$$

Further details about the noise model of the GP, training, and using prior information can be found in Appendix 1. In addition to information on cell numbers, however, we wish to incorporate information about the process cost of x. Therefore, we formulate a cost function $c(x) = c_{min} + \sum_{j=1}^{p} c_j x_j$ where c_j is a scaled marginal cost of each media component whose coefficients can be found in Table 1.

2.4.2 | BO acquisition function

To maximize media utility, we wish to maximize y(x) while minimizing cost c(x) for the highest-fidelity IS. Therefore, we posed this multiobjective optimization problem as a single-objective in the form of a desirability function D(x) (Akteke-Ozturk et al., 2018) where cell number and cost are scaled as $\overline{y}(x) = \frac{y(x) - y_L}{y_H - y_L}$ and $\overline{c}(x) = \frac{c(x) - c_H}{c_L - c_H}$ respectively.

$$D(x) = \phi(x) \sqrt{\bar{y}(x)^* \bar{c}(x)}, \tag{5}$$

where $\phi(x) = 1^*\{y(x) \ge y_L\}$ is a feasibility indicator function that is non-zero when the predicted y(x) is greater than or equal to some minimum cell number metric y_L . We set $y_L = 0.5$ and $y_H = 2.0$ to

exclude media that fail to be 50% as proliferative as the control media to preferentially select high-performance media. We scale c(x) as a "smaller-the-better" metric where $c_L = c_{min}$ and $c_H = c_{min} + \sum_{j=1}^{p} c_j$ so that we may solve our new cost-aware objective function as a single-objective problem $x^* = argmax D(x)$.

With a predictive multi-IS GP modeling $\mu(x) \approx y(x)$ and computing D(x) from Equation (5), we can use it to suggest optimal media conditions x^* . However, because we would like to solve for some optimal group of q > 1 experiments X^* rather than a single q = 1 experiment x^* (it is much more efficient to run multiple experiments at a time), we pose the optimization problem as a p^*q -dimensional multi-point optimization problem $X^* = argmax D(X)$ for multiple optimal media conditions at once. This formulation (i) does not consider uncertainty when quantifying the value of a particular set of media components and (ii) does not have an analytical form. We solved both problems by using the multi-point expected improvement function $\alpha(X)$ (Wang et al., 2020).

$$\alpha(X) = E\{(\max\{D(X)\} - D^*(X_N))^+\},\$$

where $D^*(X_N)$ is the D(x)-optimal desirability of the N points collected and $\max\{D(X)\}$ is the D(x)-optimal desirability of the q points X evaluated by $\alpha(X)$. If $\max\{D(X)\} - D^*(X_N) \le 0$ (no improvement from evaluating X) then the "+" operator sets the improvement of the design to $\alpha(X) = 0$. Thus, with $\alpha(X)$ we can quantify the value of multiple points X rather than just a single point x. Evaluating α for any group of experiments X requires further mathematical treatment, which can be found in Appendix 2.

2.4.3 | BO algorithm

The BO algorithm that designs optimal experiments is shown in Figure 1. After collecting some initial data, the multi-IS GP is trained and X^* found using multistart L-BFGS-B for some q maximum allowable number of experiments (based on laboratory constraints). The L-BFGS-B optimizer was chosen because it performs well on high dimensional problems, can be ran with multiple restarts thus improving its global optimization capabilities, and has access to gradients and Hessian approximations thus reducing computational time. Because we want to optimize the high-fidelity IS (long-term growth as Passage 2) all calculations in the BO algorithm are done using the high-fidelity IS prediction. With X^* in hand, we now must find the optimal IS to sample. We start by defining the number of high-fidelity samples we are willing to measure $q_0 < q$, with the remaining $q - q_0$ being low-fidelity IS (Figure 2).

We can pose the IS-allocation problem as "which q_0 designs in X^* has the highest $\alpha(x)$ in combination"? This requires calculating $\alpha(x)$ for all combinations $\begin{pmatrix} q \\ q_0 \end{pmatrix}$ in X^* , and allocating the highest-fidelity budget to the dominant combination. The remaining $q-q_0$ experiments can be allocated to low-fidelity IS. New experiments are

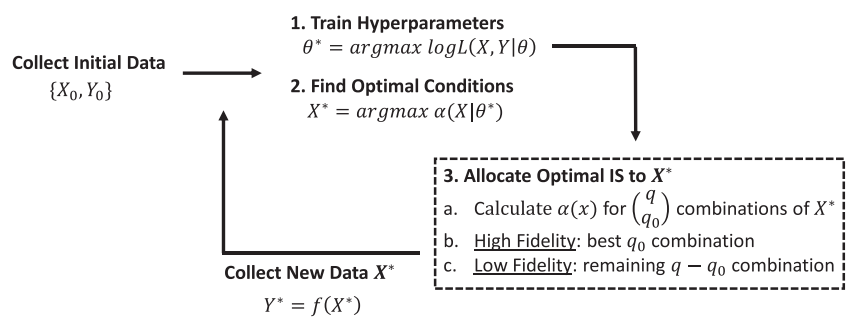


FIGURE 1 BO algorithm. This loop describes the Bayesian Optimization algorithm to maximize some acquisition function $\alpha(x)$ for a process Y = f(X) given q_0 high-fidelity IS and $q - q_0$ low-fidelity IS samples per batch of experiments. After each batch, the process is repeated until process is optimized or resources are exhausted. BO, Bayesian optimization

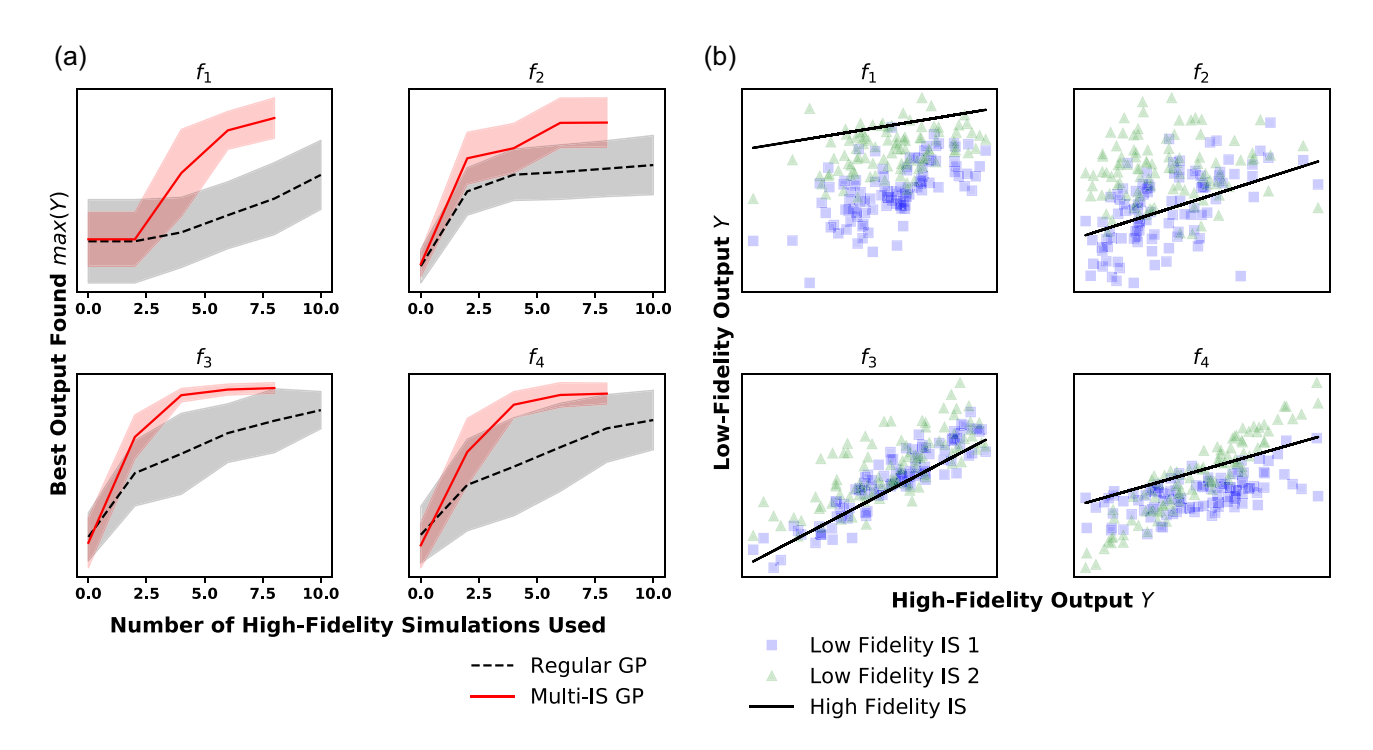


FIGURE 2 Simulation results. (a) Number of cumulative high-fidelity simulations used plotted against average (with standard deviation for five runs of the entire optimization loop) optimal output from f across five sequential iterations of the optimization framework. The multi-IS GP (solid) had access to q = 15 total simulations with $q_0 = 2$ high-fidelity and $q - q_0 = 13$ low fidelity simulations per iteration (multi-IS GP has stopped one iteration early to reduce computational burden). The regular GP (dotted) only had access to the $q_0 = 2$ high-fidelity simulations per iteration. Each test function $\{f_1, f_2, f_3, f_4\}$ had two biased low-fidelity versions whose correlations are described by plots (b). Squares and triangles represent a given f_{bias1} and f_{bias2} respectively. The solid line represents the underlying high fidelity IS f. Hyperparameter and acquisition function optimization was done using multistart L-BFGS-B implemented in botorch/scipy.

collected using the IS and component concentrations found, and the procedure looped until the process was optimized to satisfaction or resources are exhausted.

We started our BO method by initialization with 10 experiments according to Latin Hypercube design similar to (Poloczek et al., 2017) (10 experiments being the approximate capacity of our laboratory at any given time). The algorithm allocates q=10 experiments with $q_0=3$ high-fidelity IS and $q-q_0=7$ low-fidelity IS using the combinatorial heuristic described above for the optimal group X^* . This was repeated seven times, with iterative training and optimization stages to improve our model while simultaneously find optimal media. After 80 experiments (we

stopped after exhausting our cell bank) a final high-fidelity IS experiment was performed at the theoretical optima argmax D(x), for 81 experiments total.

2.5 | Computational environment and packages

Hardware used: Dell Precision 5820 Tower, Intel Xeon W-2145 DDR4-2666 Processor (3.7 GHz), 32 GB Memory. Software used: python 3.9.7 (for all programming), gpytorch 1.3.0, pytorch 1.8.1, and botorch 0.4.0 (for modeling and Bayesian optimization), pydoe 0.3.8 (for initialization using Latin Hypercube experiments).

3 | RESULTS

3.1 | Computational validation of BO method

Before optimizing our experimental system, we tested the BO algorithm on various multi-information source mathematical test functions $\{f_1, f_2, f_3, f_4\}$ (Appendix 3) solving argmax f(x) using the nosey expected multi-point improvement acquisition function on a 10-dimensional problem. Each f had two low-fidelity test functions (f_{bias1} and f_{bias2}) which differed substantially from the true test function. Given an extremely limited high-fidelity budget (10 simulations at two per iteration of the optimization loop), the multi-IS GP saw better average performance (higher outputs) compared to a regular GP with otherwise the same model architecture (hyperparameters, training method, priors, etc.). The major limitation of this experiment is that these test functions do not represent the true biological process. However, as the test functions were created to mimic noisy biological processes, we should be able to differentiate the performance of optimization methods using these results.

3.2 | Experimental validation of BO method

We then applied our BO method to C2C12 media optimization design problem. The BO method achieved a maximum desirability of

D(x) = 0.94 in 81 total experiments while the DOE only achieved a maximum at D(x) = 0.40 requiring 132 experiments. This represented a 132% improvement over the DOE and a 113% improvement over the control DMEM with 38% fewer experiments. The optimal BO medium corresponds to y(x) = 2.82 cell number with cost c(x) = 8.22, or a 227% improvement in cell number over DOE at a 34% increase in cost, and a 181% improvement in cell number over the DMEM control at a mere 1.6% increase in cost. As seen in Figure 3a the BO method also found a suboptimal medium, with higher D(x) than DOE and the DMEM control, within 30 experiments, or a 77% reduction in experimental effort.

Table 3 shows the media concentrations resulting from the BO and DOE methods along with the DMEM control used throughout this study. The BO method found that transferrin, glutamine, progesterone, and estradiol should be at a high relative concentration. Ascorbic acid, hydrocortisone, and dexamethasone should be at a low/zero concentration. The remaining components should be somewhere in between the two extremes. The DOE method, using only AlamarBlue, used a PB screening design (32 experiments) to reduce the problem size from 14 components to four, finding that glucose, glutamine, albumin, and FBS had the highest positive effect on D(x). Next, four sequential BB designs (25 experiments each), with bounds shifting in the direction of D(x)-steepest accent after each BB, used 100 experiments to find the optimal bounds of the four-dimensional factor space. Optimal factors were predicted to be nearly identical to the DMEM control, resulting in nearly

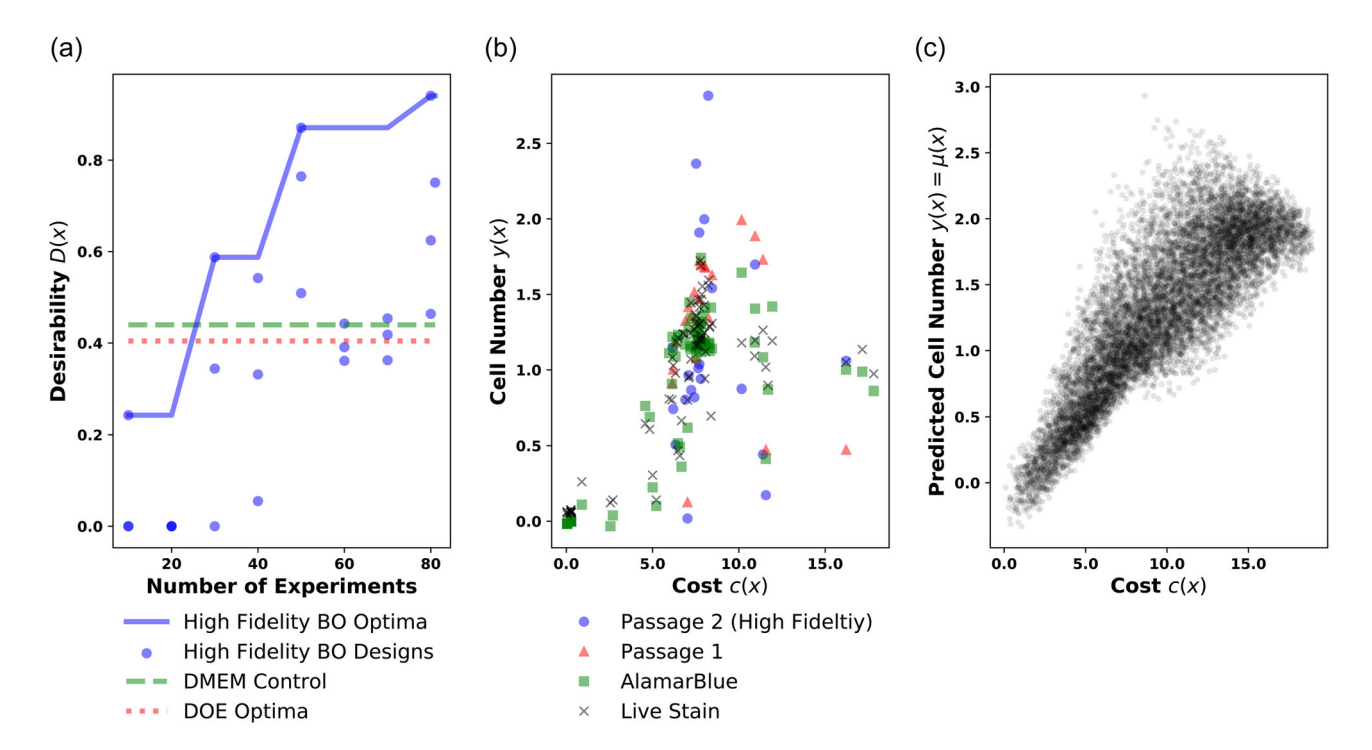


FIGURE 3 Learning curve and trade-off curve of BO method. (a) Learning curve of D(x) shows BO and DOE method designing experiments over the course of the optimization study. The line and dots represent the high-fidelity IS optima and designs, the dashed and dotted lines represent the DMEM control and DOE optima values for D(x) respectively. Each IS experiment is shown in (b) the trade-off curve indicating a clear tradeoff between cost c(x) and cell number y(x), where the dots, triangles, squares, and "x's" represent Passage 2, Passage 1, AlamarBlue, and Live Stain respectively. (c) Simulated trade-off curve also shown for high-fidelity IS also showing a predicted parabolic relationship between competing objectives y(x) and c(x). BO, Bayesian optimization; DMEM, Dulbecco's modified Eagle's medium; DOE, design-of-experiments

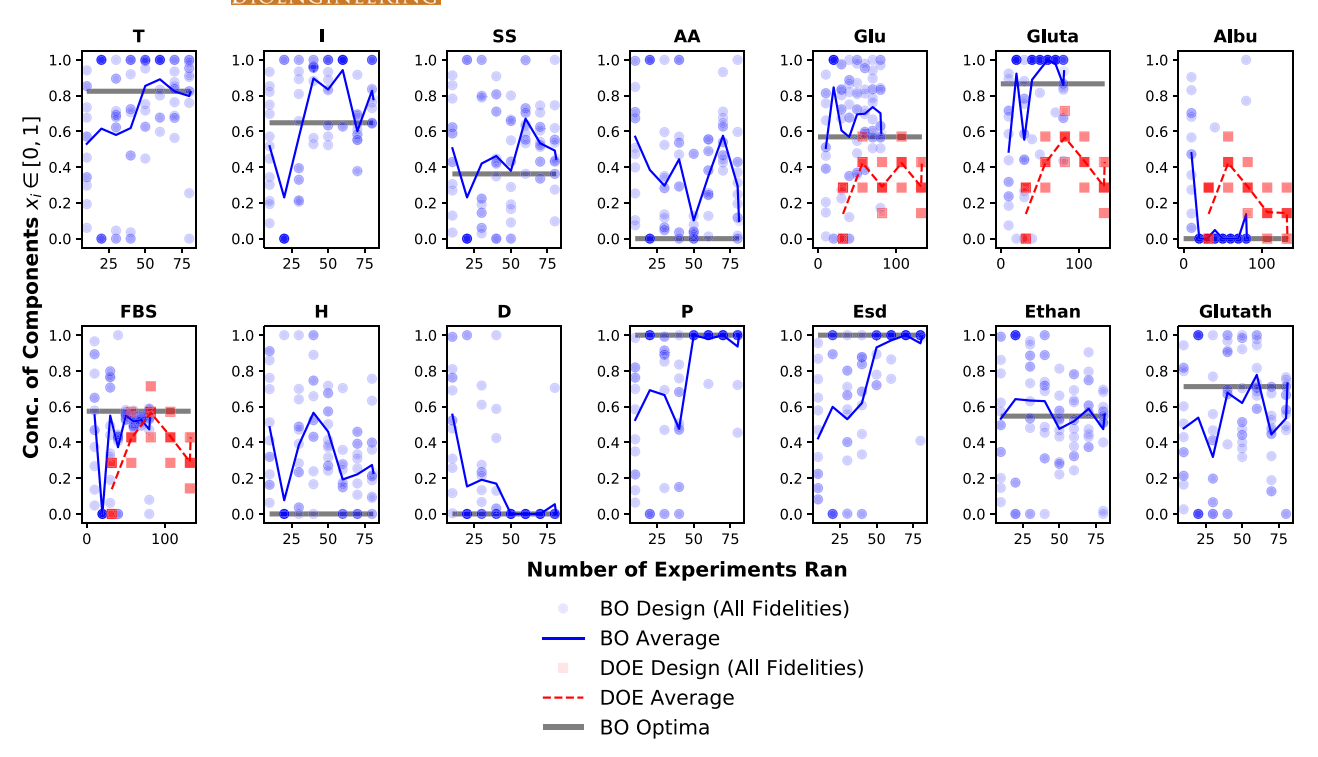


FIGURE 4 Learned optimal concentration. The conditions of each experiment (concentration ranges in Table 1) are shown plotted as a function of the cumulative number of experiments in the BO (circle) and DOE (box) study. The moving average (solid and dashed line for BO and DOE respectively) shows how each method searches for optimal concentrations. The horizontal line represents the final BO optimal concentration. BO, Bayesian optimization; DOE, design-of-experiments

identical desirability (D(x) = 0.40 vs 0.44 for DOE and DMEM control, respectively).

As expected, there was a trade-off between a number of cells y(x) and medium-cost c(x) captured in Figure 3b,c. More nutrients, especially FBS, improved cell number at the expense of higher cost; this trend then breaks down as more FBS and Albumin have a deleterious effect on growth.

We also note from Figure 4 that the BO algorithm found the optimal concentration of some components faster than others, as indicated by heavier clustering of datapoints. This is a function of how confident the multi-IS GP was in certain regions of the design space, with denser sampling being indicative of higher confidence in improvement.

3.3 | Experimental validation of long-term cell number objective function

The robustness of the multi-IS GP model was evaluated by resampling the optimal BO medium which had a cell number metric of $y^* = 2.8 \pm 0.29$. When measured again the cell number metric was $y^* = 2.7 \pm 0.93$, indicating measurement and overall system reproducibility. Next, all four optimal media were cultured for 288 total hours (to Passage 4 with 72 h/passage), to determine how well our high-fidelity IS generalized to longer-term growth. The optimal medium designed by the BO method outperformed the DOE and

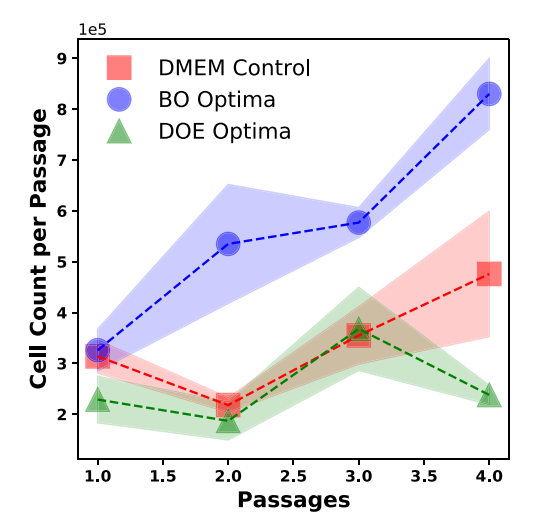


FIGURE 5 Long-term validation of optima media. The optimal BO-designed (dots), DOE (triangles), and DMEM control (squares) media performance up to Passage 4 Each passage was 72 h of growth at 37°C and 5% CO₂. Trypsinization took place after each 72 h period to count cells and replate them to allow for further growth (standard deviations indicated). The BO method designed an optimal media with substantially improved long-term growth capacity than the DOE or DMEM control. BO, Bayesian optimization; DMEM, Dulbecco's modified Eagle's medium; DOE, design-of-experiments

DMEM control substantially in a number of cells grown at Passage 4, with results summarized in Figure 5.

3.4 | Sensitivity analysis

We then examined the first and second-order effects of each component as predicted by the multi-IS GP (training on all N = 81 datapoints). Most components show a parabolic effect in both y(x) and D(x) (Figure 6), where the optimal medium is in the middle of the factor space, often in sample dense regions.

To quantify the magnitude of the predicted global effect of each component, we employ the VARS method (Razavi & Gupta, 2016a, 2016b) of sensitivity analysis because standard methods of sensitivity analysis cannot capture the "importance" of a given factor in the presence of nonlinear effects. In VARS we defined |N(h)| as the number of pairs in a set such that all possible pairs of points x^A and x^B are separated by a normalized factor distance h. We then integrated the variance $r = (y(x^A) - y(x^B))^2$ of all pairs separated by h to get the variogram $\gamma_i(h) = 1/2|N(h)|\Sigma_{(i,j)\in N(h)}r_{i,j}$. If we set h = 0.1 (10% of total normalized factor space for a given component) we are estimating a

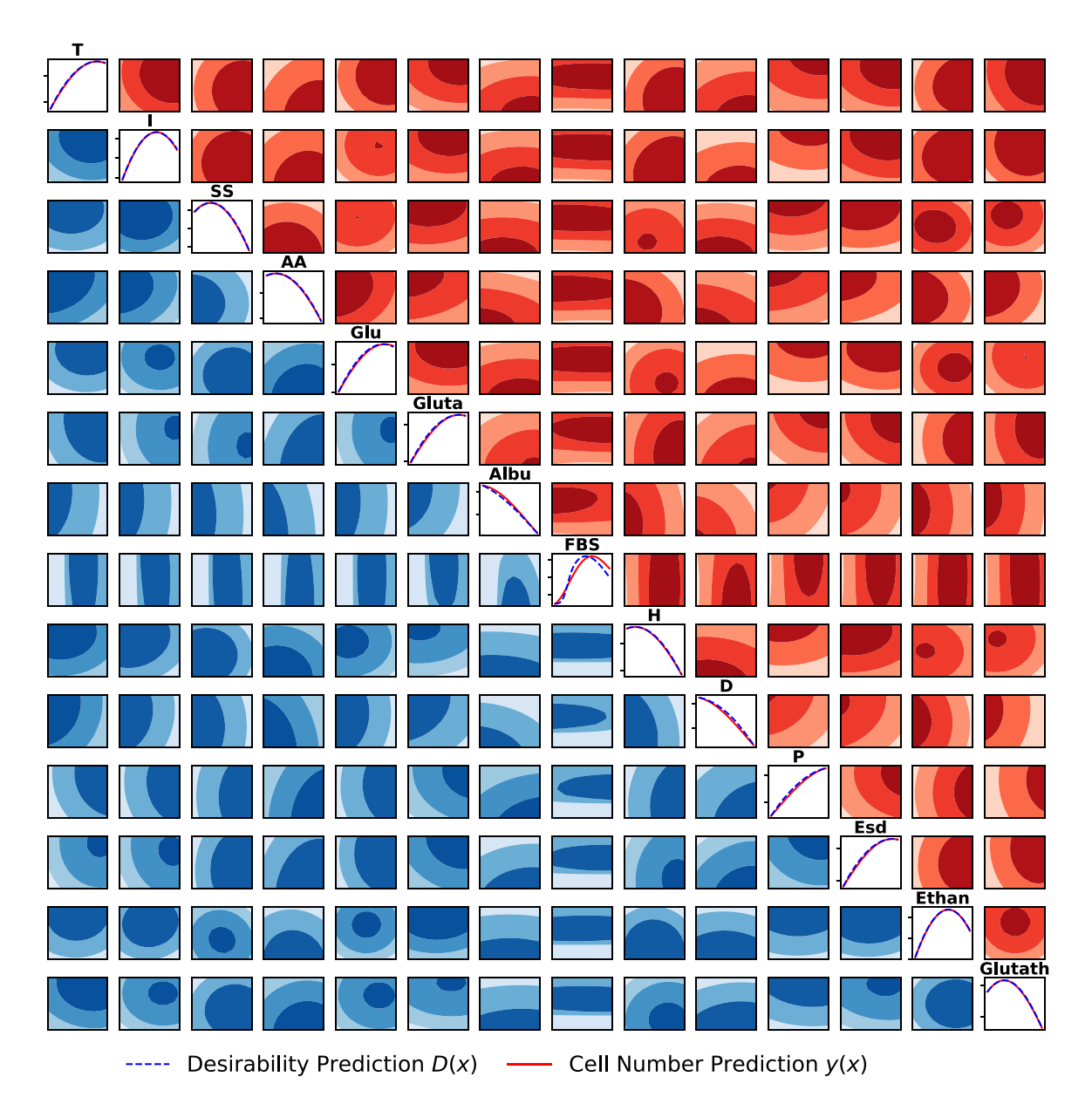


FIGURE 6 Predicted first and second-order effects. First-order predicted effects of each component of the high-fidelity IS are shown on diagonal plots (y-axis is not to scale) with solid and dashed lines representing predicted cell number y(x) and desirability D(x) respectively. The "above" diagonal plots are second-order plots for cell number y(x) and "below" are those for desirability D(x). The range of all components as described in Table 1. Labels are left off for clarity; to find the axis labels read the x-axis labels horizontal from the diagonal label and read the y-axis labels vertical from the label.

"local" variability in the output y whereas h = 0.9 would be an estimate of the "long-range" effect. Figure 7 shows these variograms γ_i for each component integrated to their "local," "medium," and "global" ranges, showing albumin, FBS, dexamethasone, and glutamine have the largest effect on D(x), with FBS being by far the most critical component.

It was also useful to examine the correlations between different IS. The model predicts all IS to have very linear

correlations (Figure 8c), while Passage 1, having the most experimental noise, had the weakest inter-IS correlations. Biases are predicted at the upper end of the output range as indicated by the deviation from the 45° line in Figure 8c. This fact is also evident in the predicted kernel matrix in Figure 8b, where the more error-prone Passage 1 data displays high off-diagonal intra-IS correlation, and the other IS show nearly identical inter and intra-IS correlations.

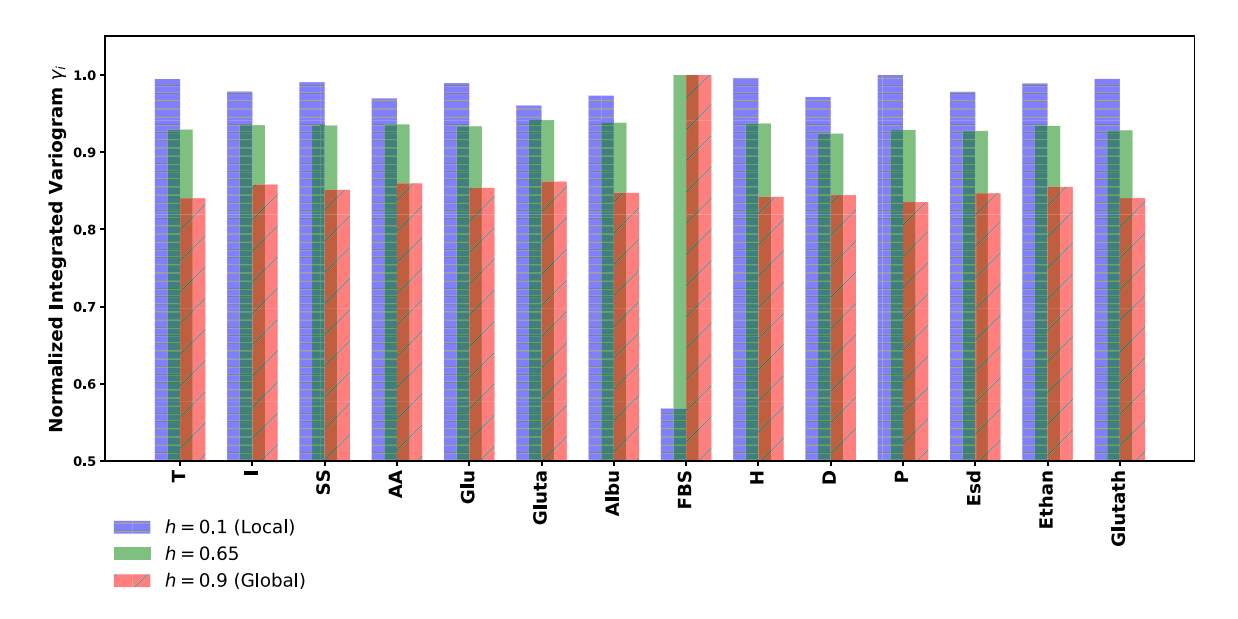


FIGURE 7 Variogram sensitivity analysis. The local (horizontal hatching), global (diagonal hatching), and mid-range sensitivity of each component on D(x) is indicated by the height of the bars. Albumin, FBS, dexamethasone, and glutamine have the largest effect on D(x), with FBS being by far the most critical component with respect to global sensitivity. Predicted variogram γ_i for each component was formed from R=300 random samples from domain [0,1]. FBS, fetal bovine serum.

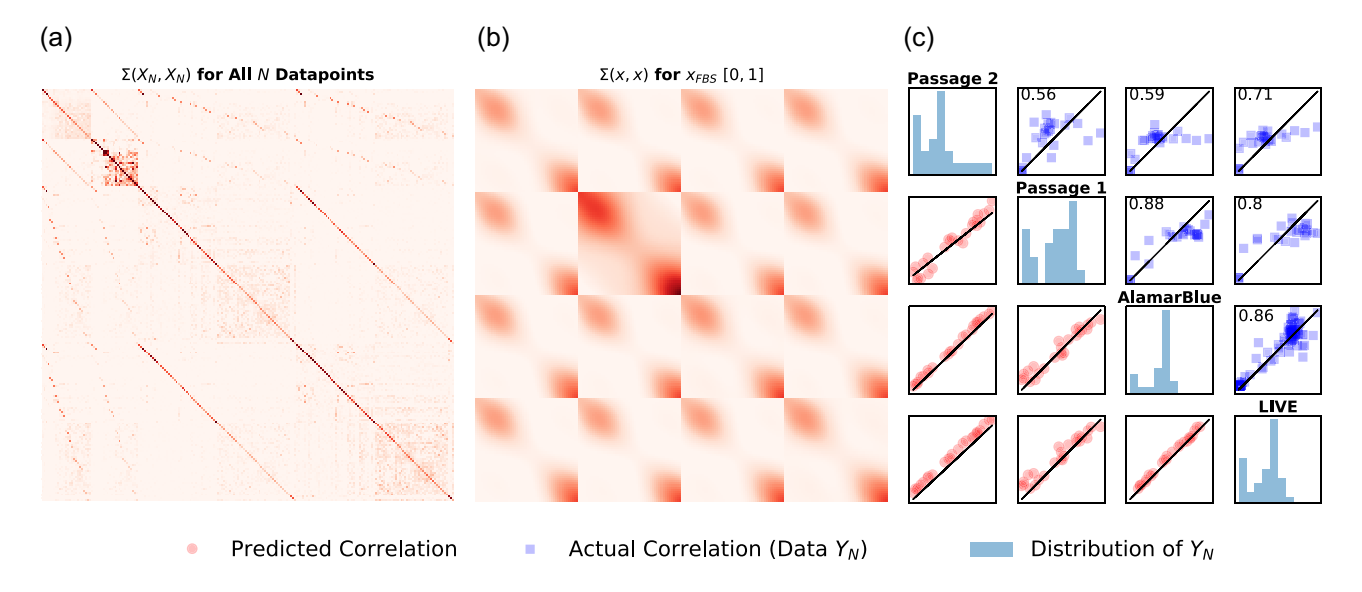


FIGURE 8 Kernel plots and IS distributions. (a) and (b) Show the output of the kernel $\Sigma(x_m, x'_{m'})$ for all data collected $\{X_N, Y_N\}$ and a simulated data set where only x_{FBS} is varied from [0,1], respectively. Darker regions indicate large values of Σ , and thus a correlation. Also (c) the various IS cell number/correlate distributions (diagonal histograms) are shown. Above the diagonal (squares) are the actual inter-IS correlations for each IS with their respective R^2 values, and below the diagonal (circles) are the predicted inter-IS correlations for a random data set.

4 | DISCUSSION AND CONCLUSION

Production scale cellular agricultural processes will require >10 passages of cell growth (O'Neill et al., 2021) so optimizing growth based on single-passage information is not adequate (Cosenza et al., 2021). However, multipassage growth assays are difficult/ expensive to measure, and even more difficult to optimize when given many components. We managed this complexity by coupling long-term (i.e., >1 passages) cell number measurements with simpler but less valuable rapid growth chemical assays (single passage) in murine C2C12 cultures as a model system for cellular agricultural applications, capturing a more wholistic model of the process. We combined this with an optimization algorithm that efficiently allocates laboratory resources toward solving argmax D(x) for desirability function D(x), a function that incorporates both cell growth and medium cost. This resulted in a 38% reduction in experimental effort, relative to a comparable DOE method, to find a media 227% more proliferative than the DMEM control at nearly the same cost. As the longer-term passaging study suggests, our Passage 2 objective function and IS were well-calibrated to mimicking the complex industrial process of growing large batches of cells over many passages, with Passage 4 cell numbers well-predicted by this objective function.

The reasons for the success of the BO are myriad. The BO method iteratively refines a single process model to improve certainty in D(x)-optimal regions, whereas the DOE relies on a series of BB designs where the older data sets are ignored because they were outside of the optimal factor space. The BO also used a variety of IS, whereas the DOE only used a single low-fidelity AlamarBlue metric (as is common in analysis of growth media). Looking at Figure 8c, the AlamarBlue and LIVE tended to cluster around the point y = 1, making it difficult to distinguish between high-quality and low-quality media. This may be due to the deviation of linearity of the %AB and F_{530} metric at high biomass. The BO method also refined its multi-IS model over the entire feasible design space, allowing it to take advantage of optimal combinations and concentrations of all 14 components over the entire domain, whereas the DOE needed to reduce the design and factor spaces to reduce the number of experiments needed, and may have identified the wrong optimal boundary locations resulting in suboptimal experimental designs. The BO method was also able to leverage information about process uncertainty to improve the model is poorly understood regions of the design space, whereas the steepest accent method used by the DOE chased after improved D(x) with little regard for overall noise or experimental errors. This was worsened by the sensitivity of the polynomial model to random inter-batch fluctuations in %AB, which may have driven the DOE to suboptimal media. Note that the success of our BO method should not be taken as generic superiority over all potential instantiations of DOE or commercial media used for C2C12 growth.

While the BO method worked well at solving the experimental optimization problem, the multi-IS GP accuracy was limited to highly sampled regions of the design space, thus limiting the efficacy of

sensitivity analysis. This was a conscious decision made to trade off postfacto analysis for sampling media with high desirability D(x). Accuracy was also limited by the low amount of data N available relative to the large dimensionality p, which is inherently the case in complex biological experiments where each batch of q experiments takes >1 week to evaluate. Finally, the hyperparameters θ^* used in the multi-IS squared exponential kernel were deliberately regularized with prior distributions to smooth the posterior of the prediction $\mu(x)$. Regularization may have diminished the quality of the inter-IS correlations; the model hyperparameters ignored features where IS differed in favor of a simpler correlative structure to explain the data. This is seen in Figure 8b,c, where the kernel evaluations show nearly equal inter-IS correlative strength for most IS used. This may have "squished"/ignored features that could have provided additional information, but at the cost of sampling the design space too widely, again a deliberate choice of model skepticism towards outliers.

Even with these limitations, the BO method clearly performs well on media optimization systems relevant to cellular agriculture, that is, those with multiple and potentially conflicting information sources with varying levels of difficulty in measuring. The media resulting from the BO algorithm supported significantly more C2C12 cell growth with only a small increase in cost. This algorithm performs better than traditional DOE in this case, especially in incorporating critical data from growth after the multiple passages in an affordable manner. With these results, it should be possible to implement this type of experimental optimization algorithm in other systems of importance to cellular agriculture and cell culture production processes with difficult-to-measure output spaces, including for optimization of serum-free media for cell growth and for differentiation.

ACKNOWLEDGMENT

We thank New Harvest and the Good FoodInstitute, along with a NSF Growing Convergence grant (2021132), for funding this study.

DATA AVAILABILITY STATEMENT

The data that support the findings of this study are openly available in Zachary Cosenza's Github at https://github.com/ZacharyCosenza/GradStuff_Cosenza.

ORCID

Zachary Cosenza http://orcid.org/0000-0002-3944-7948 David E. Block http://orcid.org/0000-0003-1582-6641

REFERENCES

Akteke-Ozturk, B., Koksal, G., & Weber., G. W. (2018). Nonconvex optimization of desirability functions. *Quality Engineering*, 30(2), 293–310. https://doi.org/10.1080/08982112.2017.1315136

Ankenman, B., Nelson, B. L., & Staum., J. (2010). Stochastic kriging for simulation metamodeling. *Operations Research*, 58(2), 371–382. https://doi.org/10.1287/opre.1090.0754

Belakaria, S., Deshwal, A., & Doppa, J. R. (2019). Max-value entropy search for multi-objective Bayesian optimization. *Advances in Neural Information Processing Systems*, 32(NeurIPS).

- Brunner, D., Appl, H., Pfaller, W., & Gstraunthaler, G. (2010). Serum-free cell culture: the serum-free media interactive online. *Database*, 27(December 2009), 53–62.
- Coleman, M. C., & Block, D. E. (2006). Bayesian parameter estimation with informative priors for nonlinear systems, *AIChE Journal*, *52*(2), 651–667. https://doi.org/10.1002/aic.10667
- Cosenza, Z., Block, D. E., & Baar, K. (2021). Optimization of muscle cell culture media using nonlinear design of experiments, *Biotechnology Journal*, 16(11), 2100228. https://doi.org/10.1002/biot.202100228.
- Cosenza, Z., & David, E. B. (2020). A generalizable hybrid search framework for optimizing expensive design problems using surrogate models. *Engineering Optimization*. 0305215X.2020.1826466.
- Jian, W., & Frazier, P. I. (2018). Continuous-fidelity bayesian optimization with knowledge gradient (Nips 2017): 1-10.
- Kolkmann, A. M., et al. (2020). Serum-Free Media for the Growth of Primary Bovine Myoblasts. Cytotechnology, 72(1), 111–120. https:// doi.org/10.1007/s10616-019-00361-y
- Kotthoff, L., Wahab, H., & Johnson, P. (2021). Bayesian Optimization in Materials Science: A Survey: 1–15. http://arxiv.org/abs/2108.00002.
- Letham, B., Karrer, B., Ottoni, G., & Bakshy, E. (2019). Constrained Bayesian optimization with noisy experiments. *Bayesian Analysis*, 14.
- O'Neill, E. N., Cosenza Z. A., Baar, K., & Block, D. E. (2021). Considerations for the development of cost-effective cell culture media for cultivated meat production. *Comprehensive Reviews in Food Science and Food Safety*, 20(1), 686–709.
- Poloczek, M., Wang, J., & Peter, I. F. (2017). Multi-information source optimization. Advances in Neural Information Processing Systems.
- Razavi, S., & Gupta, H. V. (2016a). A new framework for comprehensive, robust, and efficient global sensitivity analysis. *Theory Water Resources Research*, 52(1), 423–439. https://onlinelibrary.wiley.com/doi/abs/10.1002/2015WR017558
- Razavi, S., & Hoshin, V. G. (2016b). A new framework for comprehensive, robust, and efficient global sensitivity analysis: 2. Application. Water Resources Research, 52(1), 440–455. https://onlinelibrary.wiley.com/doi/abs/10.1002/2015WR017559
- Schulz, E., Speekenbrink, M., & Krause, A. (2018). A tutorial on Gaussian process regression: modelling, exploring, and exploiting functions. *Journal of Mathematical Psychology*, 85, 1–16. https://doi.org/10.1016/j.jmp.2018.03.001
- Shu, L., Jiang, P., & Wang, Y. (2021). A multi-fidelity Bayesian optimization approach based on the expected further improvement. *Structural and Multidisciplinary Optimization*, 63(4), 1709–1719. http://link.springer.com/10.1007/s00158-020-02772-4

- Singh, V., Haque, S., Niwas, R., Srivastava, A., Pasupuleti, M., & Tripathi, C. K. M. (2017). Strategies for fermentation medium optimization: An in-depth review. Frontiers in Microbiology, 7, 1–16. http://journal.frontiersin.org/article/10.3389/fmicb.2016.02087/full
- Takeno, S., Fukuoka, H., Tsukada, Y., Koyama, T., Shiga, M., Takeuchi, I., & Karasuyama, M. (2019). Multi-Fidelity Bayesian Optimization with Max-Value Entropy Search. arXiv.
- Tracey, B. D., & Wolpert, D. H. (2018). Upgrading from Gaussian processes to student's-T processes. AIAA Non-Deterministic Approaches Conference, (209969).
- van der Valk, J. (2018). Fetal bovine serum (FBS): Past present future. ALTEX: Alternativen zu Tierexperimenten, 35(1), 99–118. https://www.altex.org/index.php/altex/article/view/101
- Wang, J., Clark, S. C., Liu, E., & Frazier, P. I. (2020). Parallel Bayesian global optimization of expensive functions. *Operations Research*, 68(6), 1850–1865. http://pubsonline.informs.org/doi/10.1287/opre. 2019.1966
- Zhang, G., & Block, D. E. (2009). Using highly efficient nonlinear experimental design methods for optimization of *Lactococcus lactis* fermentation in chemically defined media, *Biotechnology Progress*, 25(6), 1587–1597 https://onlinelibrary.wiley.com/doi/10.1002/btpr.277.
- Zhang, G., Mills, D. A., & Block, D. E. (2009). Development of chemically defined media supporting high-cell-density growth of Lactococci, Enterococci, and Streptococci. Applied and Environmental Microbiology, 75(4), 1080–1087.
- Zhang, G., Olsen, M. M., & Block, D. E. (2007). New experimental design method for highly nonlinear and dimensional processes, AIChE Journal, 53(8), 2013–2025. https://onlinelibrary.wiley.com/doi/10. 1002/aic.11226.

SUPPORTING INFORMATION

Additional supporting information can be found online in the Supporting Information section at the end of this article.

How to cite this article: Cosenza, Z., Astudillo, R., Frazier, P. I., Baar, K., & Block, D. E. (2022). Multi-information source Bayesian optimization of culture media for cellular agriculture. *Biotechnology and Bioengineering*, 119, 2447–2458. https://doi.org/10.1002/bit.28132